Article

Photoluminescent Investigation of the Doping Site of Eu³⁺-Doped [Zn₃(BTC)₂·12H₂O] Metal-Organic Framework Prepared by Microwave-Assisted Hydrothermal Synthesis

César S. Cunha,[a] Oscar L. Malta, [b] Huayna Terraschke [,c] and Hermi F. Brito [*,a]*

*[a]Instituto de Química, Universidade de São Paulo, Av. Prof Lineu Prestes, 748,
05508-000 São Paulo-SP, Brazil*

*[b]Departamento de Química Fundamental, Universidade Federal de Pernambuco,
50670-901 Recife-PE, Brazil*

*[c]Institut für Anorganische Chemie, Christian-Albrechts-Universität zu Kiel, Max-Eyth-Str. 2,
24118 Kiel, Germany*

The [Zn₃(BTC)₂·12H₂O] (BTC = 1,3,5-tricarboxylate) metal-organic framework (MOF) was successfully synthesized using a microwave-assisted hydrothermal synthesis technique, which allowed for significantly decreased reaction time compared to the production of the same compound via conventional heating. *In situ* doping with Eu³⁺ ions at concentrations ranging from 1.0 to 5.0 mol% produced doped materials whose emission ranged from blue to red color. The Eu³⁺ spectroscopic properties were used to study the incorporation of the dopant into the structure of [Zn₃(BTC)₂·12H₂O], even at very low concentrations. These experiments confirmed the usefulness of this ion as a luminescent probe, as it permitted the identification of small variations in structure not perceptible by X-ray diffraction. The variation in the coordination environment induced by increases in doping percentage was analyzed by evaluating changes in the characteristic Eu³⁺ excitation and emission profiles, using them to calculate luminescence lifetimes, experimental intensity parameters Ω_λ (λ: 2 and 4) as well as the intrinsic quantum yield ($Q_{Eu^{3+}}^{Eu^{3+}}$) of the $^5D_0$ emitting level of each doped MOF. The excitation and luminescence spectra show that intramolecular energy transfer from the BTC linker to Eu³⁺ ion, and we could observe the emission color tuning originated from the emissions of the BTC ligand and Eu³⁺ ion.

Keywords: metal-organic framework, luminescence, Eu³⁺

Introduction

Metal-organic frameworks (MOFs) are hybrid materials consisting of isolated cations or metal clusters strongly bound by rigid and multidentate organic linkers. MOFs retain the highly crystalline structure and rigid topologies of pure inorganic solids while gaining unique physical and/or chemical properties from incorporated organic molecules.[1] Manipulation of these additional properties through functional optimization of organic linkers allows for the generation of highly tailored compounds for use in various industrial and technological applications.[2]

One of the essential parameters is the linker design that can influence the nature of the metal coordination center.

For this, functional carboxyl groups are often added to the organic structure.[3] Carboxylate groups can provide outstanding coordination stability while allowing flexibility in coordination number and structure design, as each anion is capable of forming multiple bond types with the metal center, including unidentate bonds, chelating bridges, and bidentate bridges, among others.[4] Incorporation of aromatic rings into the linker structures can increase the MOF rigidity (due to their inflexible forms) and thermostability.[3]

Conjugated π bonds in aromatic rings also allow the absorption and emission of energy by the linker, providing MOFs containing non-luminescent metal ions (commonly Zn or Cd) with luminescent properties.[5,6] Electronic transitions in organic ligands can also enhance or alter the inherent luminescent properties of metal ion centers (for example, rare earth (RE) metal ions), therefore, generating efficient luminescent MOF materials.

*e-mail: hterraschke@ac.uni-kiel.de; hefbrito@iq.usp.br

Importantly, the combination of the rigid structure, luminescent properties and unique permanent porosity qualifies these materials as a sensor for small molecules or ions. In this case, the presence of the sensed species in the porous spaces can induce emission color tuning in the MOFs systems.[5,7] This exceptional characteristic of MOFs makes them promising candidates for the development of new luminophores, biomolecule probes, photocatalysis and solid-state lighting (SSL) for luminescent devices such as organic light-emitting diodes (OLEDs), among others.[8]

One of the MOFs being investigated for possible applications in these fields is based on the [Zn$_3$(BTC)$_2$·12H$_2$O] (BTC = 1,3,5-tricarboxylate) compound. Previous works[9,10] have described the structure and geometry of this compound in detail. Its structure belongs to the monoclinic crystalline systems, space group C$_2$. The metallic ion possesses two symmetry sites, both coordinated by four water molecules. At the first site, the metal ion is coordinated in the axial position by two unidentate linkers, forming an almost perfect octahedron. The second site is coordinated by a single, equatorial bidentate linker, generating a distorted octahedron.[9,10]

Eu^{3+} ion presents characteristic narrow absorption, excitation and emission bands arising from the 4f-4f transitions, exhibiting red emission colors, and their coordination compounds can act as efficient light conversion molecular devices (LCMDs).[11] This rare earth ion is mainly used as an efficient luminescent probe due to the fact that both emitting $^5D_0$ and ground $^7F_0$ states are non-degenerate as well as the radiative rate of the $^5D_0 \rightarrow$ $^7F_1$ transition is allowed by the magnetic dipole mechanism and, therefore, is virtually insensitive to the chemical environment around the metal ion.[12]

In this work, we present evidence that microwave-assisted hydrothermal synthesis represents a more efficient and effective method for the production of the [Zn$_3$(BTC)$_2$·12H$_2$O], requiring shorter reaction times and milder reactants and reaction parameters than conventional synthesis techniques while producing a more uniform and defect-free product. Additionally, for the first time, we used the Eu^{3+} ion *in situ* doping protocol to investigate the luminescence properties of the [Zn$_3$(BTC)$_2$·12H$_2$O]. The incorporation of Eu^{3+} ions into the structure of the [Zn$_3$(BTC)$_2$·12H$_2$O] matrix contributes with red color to the emission spectra of the materials. Despite the interesting luminescence properties of Eu^{3+}, its ions are not able to efficiently absorb light, due to the parity-forbidden character of their 4f $\rightarrow$ 4f electronic transitions.[2] Therefore, applying [Zn$_3$(BTC)$_2$·12H$_2$O] as host lattice allows us to profit from the so-called antenna effect, in which the

excitation light is absorbed by the BTC^{3-} organic ligand and transferred to the Eu^{3+} doping ions, significantly enhancing their luminescence intensity. Finally, the emission bands assigned to the $^5D_0 \rightarrow$ $^7F_{J = 0-4}$ transitions of the Eu^{3+} ion and their doping concentrations allowed to obtain information on the doping site and luminescent properties of the MOF material, which might be useful for the photonic application.

Experimental

Materials and equipment

Benzene-1,3,5-tricarboxylic acid (trimesic acid or H$_3$BTC, 95%), zinc acetate dihydrate (98-100%), and europium oxide (99.99%) purchased from Sigma-Aldrich (Darmstadt, Germany), Alfa Aesar (Ward Hill, USA) and CSTARM (Shanghai, China), respectively, were used without further purification or drying. Europium chloride (EuCl$_3$·6H$_2$O) was obtained by using an aqueous suspension of europium oxide with concentrated hydrochloric acid until the solution reached a pH ca. 6.0. The solution was then dried in a porcelain capsule over a water bath until complete solvent evaporation. The crystalline solid product was stored under reduced pressure in a vacuum desiccator until experimental use.

Elemental analysis of the hydrogen and carbon content of the synthesized products was performed using a PerkinElmer CHN 2400 (Waltham, USA) series II elemental analyzer. Infrared (IR) absorption spectra were recorded using the KBr pellet technique and utilizing a Bomem MB100 FTIR spectrometer (Zurich, Switzerland) in the spectral range from 400 to 4000 cm^{-1}. X-ray powder diffraction (XPD) patterns were recorded utilizing a Rigaku Miniflex II (Tokyo, Japan) (CuK$_{\alpha1}$, 1.5406 Å) from 5 to 60° in the 2θ with a step size of 0.05° and step time of 1.0 s. Thermogravimetry and derived thermogravimetry (TG-DTG) analyses were obtained using an sTA i 1500 (ISI Instrument Specialists Incorporated, Twin Lakes, USA) equipment in the temperature interval from 30 to 900 °C with a constant heating rate of 10 °C min^{-1} and a dynamic synthetic air flow rate of 50 cm^3 min^{-1}. Structural morphology and size of product crystals were observed using a JEOL JSM 7401F Scanning Emission Electron Field Microscope (SEM) (Tokyo, Japan). The preparation of solid samples for SEM analysis involved the production of a suspension of obtained crystal product into a solution of propanol. The obtained suspension was dripped onto a carbon support matrix and the solvent was allowed to evaporate. Inductively coupled plasma optical emission spectroscopy (ICP OES) analyses were carried out using

a Spectro Arcos spectrometer (Kleve, Germany) with an optical system sealed and purged with argon. Diffuse reflectance data were obtained utilizing a Shimadzu UV-2600 UV-VIS spectrometer with an ISR-2600 Integrating Sphere (Kyoto, Japan). Photoluminescence investigations utilized excitation and emission spectra recorded at room and liquid nitrogen temperatures (300 and 77 K, respectively) using front-face data collection mode (22.5°) and a 450 W xenon lamp excitation source coupled to a SPEX-Fluorolog 3 spectrometer (HORIBA Jobin Yvon, Kyoto, Japan) with 0.22 m double monochromators. Luminescence decay was investigated using a SPEX 1934D phosphorimeter (HORIBA Jobin Yvon, Kyoto, Japan) accessory attached to a 150 W pulsed xenon lamp. Time-resolved emission spectra were obtained using a xenon flash lamp based Varian/Agilent CARY Eclipse fluorescence spectrophotometer (Santa Clara, USA). Phosphorescence was measured with a preset delay and gate times of 0.1 and 10 ms, respectively.

Synthesis of Eu^{3+}-doped and nondoped [Zn$_3$(BTC)$_2$·12H$_2$O] MOF by hydrothermal method with microwave-assisted heating

For the preparation of nondoped [Zn$_3$(BTC)$_2$·12H$_2$O], benzene-1,3,5-tricarboxylic acid (H$_3$BTC, 0.8 mmol, 0.1681 g) and zinc acetate dihydrate (Zn(Ac)$_2$·2H$_2$O, 1.2 mmol, 0.2633 g) were vigorously mixed in 12 mL of water for 10 min. For microwave-assisted heating, the solution was added in a 30 mL vial from Monowave 300, Anton Paar (Graz, Austria) and heated at 160 °C for 25 min under stirring. After cooling to room temperature, the white solid product was filtered, washed three times with 10 mL of water, dried at room temperature and sealed. The solid material is stable in air, non-hygroscopic and insoluble in common organic solvents such as acetone, dimethyl sulfoxide (DMSO), acetonitrile, chloroform, and ethanol, indicating that it can be used as optical markers, such as in banknotes and luminescent paints.

The Eu^{3+}-doped [Zn$_3$(BTC)$_2$·12H$_2$O] systems were obtained by mixing the appropriate volume of a 0.05 M EuCl$_3$·6H$_2$O aqueous solution to a Zn(Ac)·2H$_2$O solution (Table S1, Supplementary Information (SI) section). The percentage of dopant was calculated as the charge divided by the mol of the linker. The amount of Zn^{2+} cation was reduced proportionally with the increase of the Eu^{3+} cation, taking into account the difference in charge to ensure stable oxidation states for both metals. In a 30 mL reaction flask, 0.8 mmol (0.1681 g) of protonated linker BTC was added to 12 mL of water, together with the appropriate masses of Zn(Ac)$_2$·2H$_2$O and volumes of EuCl$_3$ solution in order to produce materials doped with 1.0; 1.5; 2.0; 2.5; 3.0;

3.5; 4.0 and 5.0 mol% Eu^{3+} ion (Table S1, SI section). The synthesis procedure for the doped materials was similar to the synthesis of the nondoped material. The reaction was stirred for 10 min, followed by incubation at 160 °C for 25 min. The resulting white solid was filtered, washed with water and stored under reduced pressure. These materials showed similar stability to the nondoped compound.

Results and Discussion

Confirmation of product formation and analysis of hydration status

Elemental analysis (Table S2, SI section) confirmed the product composition, with carbon and hydrogen ratios closely resembling those anticipated. The slight fluctuations from calculated ratios were due to changes in the degree of product hydration, as verified by hydration analysis using thermogravimetric curve generation in the temperature interval from 30 to 700 °C in a synthetic atmosphere (composition: 20% O$_2$ / 80% N$_2$).

Successful product synthesis was also confirmed by X-ray diffraction and thermal decomposition analyses, with the product-generated diffraction patterns that will be discussed in the next section and decomposition rates (Figure S1, SI section) closely matching those calculated for [Zn$_3$(BTC)$_2$·12H$_2$O].[9,10]

Thermal decomposition analysis of the Eu^{3+}-doped [Zn$_3$(BTC)$_2$·12H$_2$O] could also confirm both the proper formation of [Zn$_3$(BTC)$_2$·12H$_2$O] and successful incorporation of Eu^{3+} ions into the doped crystal lattice. Doped materials were found to have decomposition profiles, which strongly resembled those obtained for the nondoped compound, but that were shifted by approximately 10 °C during the final organic decomposition phase (Figure S1, SI section). This was consistent with the anticipated decreased crystal lattice stability induced by the incorporation of higher doped content of Eu^{3+} ion into the crystalline structure. This strongly indicated the successful doping of these compounds.[13]

These product parameters were unchanged when the product was synthesized using a microwave-assisted hydrothermal synthesis, indicating the successful production of the material with this method, despite cutting the synthesis time from 14 h in the conventional resistive heating method to a mere 25 min.[9,14]

Analysis of the material structure

Analysis of the infrared absorption spectra of the C=O and C−O bonds in the carboxylate group of the BTC

molecules was used to determine the linker deprotonation state and coordination orientation around the metallic center.[4,15] Figure 1 shows the infrared absorption spectra of pure BTC salt, nondoped [$Zn_3(BTC)_2 \cdot 12H_2O$] and [$Zn_3(BTC)_2 \cdot 12H_2O$] doped with 1.0; 3.0 and 5.0 mol% Eu³⁺ ions (Table S3, SI section).

The characteristic carboxylic acid bands (C=O: 1720 cm⁻¹ and C−O: 1270 cm⁻¹) were observed in the absorption spectra of the H₃BTC trimesic acid (Figure 1). In the spectra obtained from the synthesized [$Zn_3(BTC)_2 \cdot 12H_2O$] MOFs, however, these bands disappeared and new absorption peaks appeared at around 1600 and 1400 cm⁻¹, corresponding to absorption maxima typically observed for the antisymmetric and symmetric (COO⁻) stretch of a fully deprotonated carboxylate anion.[15-17] Full deprotonation of the carboxyl group in the synthesized MOFs suggested that these groups were directly coordinated to the metal ions during the [$Zn_3(BTC)_2 \cdot 12H_2O$] formation.

Direct coordination by the carboxyl groups was further suggested by the presence of bands at 1404 and 920 cm⁻¹ in the linker absorption spectra of the nondoped MOF. These unique signals indicated the segregation of COH-bonds into in-plane and out of plane bonds, distinctions only possible if the BTC molecule were anchored to the metal coordination center.[17] Besides, the broad absorption band at 3460 cm⁻¹ confirms data obtained from CHN and TG analyzes, indicating a high degree of MOF hydration. All the doped [$Zn_3(BTC)_2 \cdot 12H_2O$:Eu³⁺] and nondoped compounds, generated identical IR spectra, suggesting that doping did not significantly change the coordination structure of the MOF.

This finding was partially confirmed by powder X-ray diffraction analysis. The diffraction patterns of the MOFs doped at the four lower doping concentrations

(1.0-4.0 mol%) were highly similar to that of the nondoped MOF (Figure 2a), indicating maintenance of the original structure despite the introduction of the higher Eu³⁺ dopant concentrations. On the other hand, the [$Zn_3(BTC)_2 \cdot 12H_2O$:Eu³⁺] compound doped at 5.0 mol% generated unique reflections (marked signals) not observed in the diffractograms of the other materials, suggesting that the structure of this system was significantly affected by doping at this higher concentration.

Closer examination of the most intense reflections at 17 to 19° 2θ (Figure 2b) also revealed a minute shift towards a smaller diffraction angle for those MOFs that were doped with 1.0-4.0 mol% Eu³⁺ compared to the nondoped one. This shift is consistent with an expansion of the cell parameters resulting from the incorporation of the higher Eu³⁺ ion ionic radius into the crystalline structure, providing yet further evidence for successful doping of the [$Zn_3(BTC)_2 \cdot 12H_2O$].[8] In contrast, this trend on the shifts of the reflections of the doped [$Zn_3(BTC)_2 \cdot 12H_2O$] is not observed for the MOFs doped with 5.0 mol% Eu³⁺, most probably due to the more drastic changes in the crystal structure caused by the crystallization of an impurity phase. Unfortunately, due to low dopant concentrations, differences in the charge, radius size, and coordination sphere size between the Zn²⁺ and Eu³⁺ ions, the differences in reflection angle were not pronounced enough to determine the exact location and chemical environment around the Eu³⁺ ions by means of X-ray diffraction.

Analysis of material morphology

Scanning electron microscope images of the nondoped compound (Figure 3a) revealed a rod-shaped crystal morphology, with a diameter of 2 μm and a length
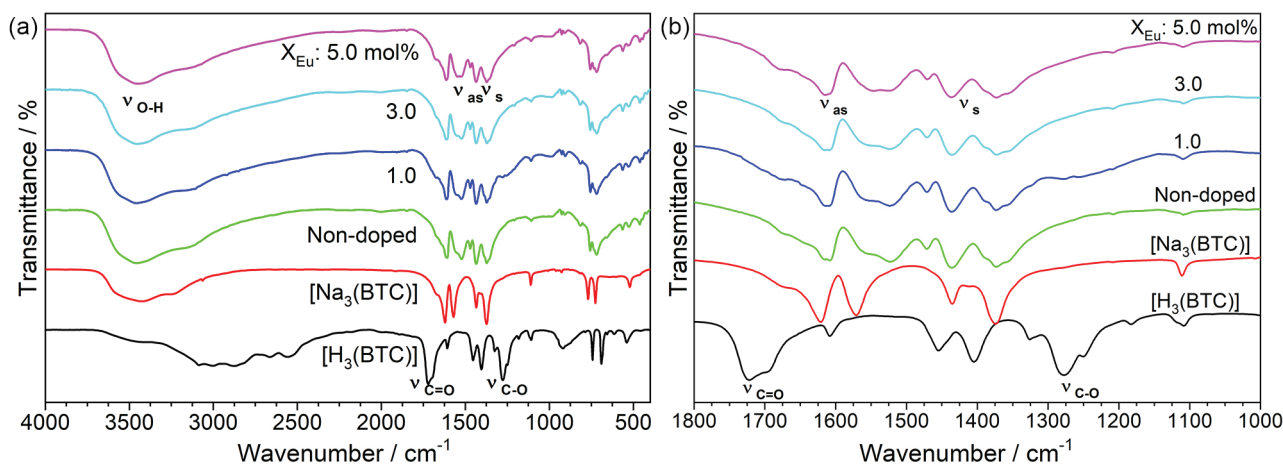
**Figure 1.** (a) Infrared absorption spectra of the H₃(BTC) (black curve), Na₃(BTC) (red curve) and [$Zn_3(BTC)_2 \cdot 12H_2O$] nondoped (green curve) and [$Zn_3(BTC)_2 \cdot 12H_2O$] doped with 1.0 (dark blue curve), 3.0 (light blue curve) and 5.0 mol% (pink curve) Eu³⁺ ions; (b) magnification at the region between 1000-1800 cm⁻¹.
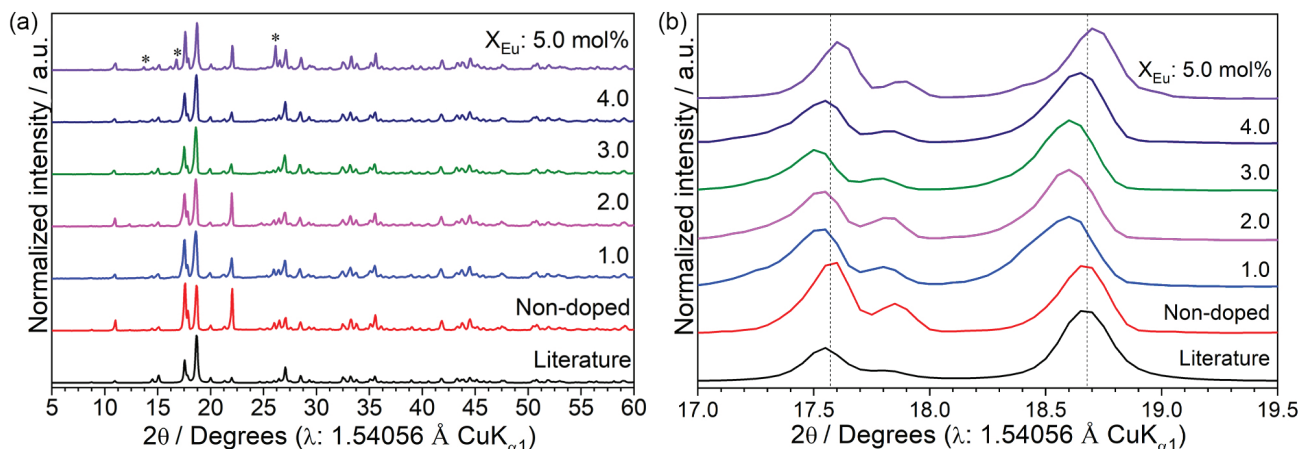
Figure 2. (a) X-ray powder diffraction, comparing the calculated diffraction pattern for $[Zn_3(BTC)_2 \cdot 12H_2O]$[9,10] (black curve) with the products synthesized by microwave-assisted hydrothermal method, nondoped (red curve) and doped with 1.0 (blue curve), 2.0 (pink curve), 3.0 (green curve), 4.0 (navy curve) and 5.0 mol% (violet curve); (b) comparison of the position of diffraction peaks at 17 and 19.5° from doped, nondoped and calculated diffraction patterns of $[Zn_3(BTC)_2 \cdot 12H_2O]$.

exceeding 30 μm. This morphology is consistent with that reported in the literature[14,18,19] for conventionally synthesized $[Zn_3(BTC)_2 \cdot 12H_2O]$ crystals, further validating successful product formation. This asymmetrical structural composition also provided an explanation for the appearance of preferential orientation reflections in the *hkl* 400 at 22° 2θ in the X-ray diffractogram (Figure 2a).
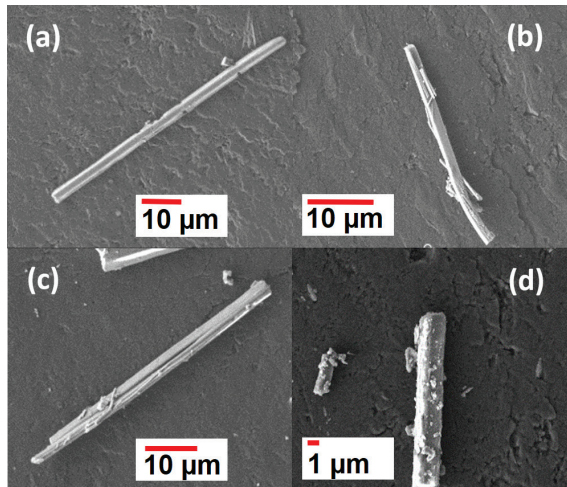
Figure 3. Scanning electron microscopy images of the compounds: (a) nondoped, and doped with (b) 1.0, (c) 3.0 and (d) 5.0 mol% Eu^{3+} ions.

$[Zn_3(BTC)_2 \cdot 12H_2O]$ matrix doped with 1.0 (Figure 3b), 2.0, 3.0 (Figure 3c) and 4.0 mol% Eu^{3+} were found to have the same rod-shaped morphology and dimensions as the nondoped compound. The 5.0 mol% doped material (Figure 3d), however, was found to have morphological differences. Scans revealed the presence of particles with indeterminate morphologies deposited on the surface of the rods. These particles indicated a phase separation or a distortion in the crystalline lattice of the material significant

enough to prevent uninterrupted crystal growth along its established axis. The presence of these particles provided a potential explanation for additional reflections observed in the diffraction patterns for this compound (Figure 2a).

Investigation of optical properties

$[Zn_3(BTC)_2 \cdot 12H_2O]$ materials were found to be highly reflective in appearance, indicating that the material was poor at absorbing radiation in the visible region of the spectrum (Figure S2, SI section). This observation was confirmed by diffuse reflectance analysis (Figure S2), which revealed reflectance above 70% for all wavelengths longer than 340 nm. This reflectance dropped abruptly as wavelengths fell below 340 nm, reaching 10% by 320 nm.

Absorption data for $[Zn_3(BTC)_2 \cdot 12H_2O]$ was analyzed via a Tauc plot.[20] The Tauc equation $((\alpha h\nu)^{1/n})$ allows calculation of the band gap of the material using absorption coefficients (α), the energy of the absorbed light $(h\nu)$, and a transition coefficient (β), where β assumes the values of 1/2 for direct phonon-assisted transitions, 2 for indirect phonon-assisted transition, 3/2 for direct forbidden transitions and 3 for indirect forbidden transitions. Analysis of absorption values for the nondoped and doped $[Zn_3(BTC)_2 \cdot 12H_2O]$ for all transition types revealed an average band gap of 4.0 eV. Table S4 (SI section) summarizes the individual band gaps calculated for each compound and transition type.

The excitation spectra of nondoped $[Zn_3(BTC)_2 \cdot 12H_2O]$ compound were recorded at 300 K temperature using excitation energy ranging from 200 to 450 nm, monitoring at 400 nm (Figure 4). The spectrum shows a broad excitation band at 350 nm assigned to the $S_0 \rightarrow S_1$ transition of the BTC ligands is dominant when monitoring at 400 nm as expected.[11,21,22]
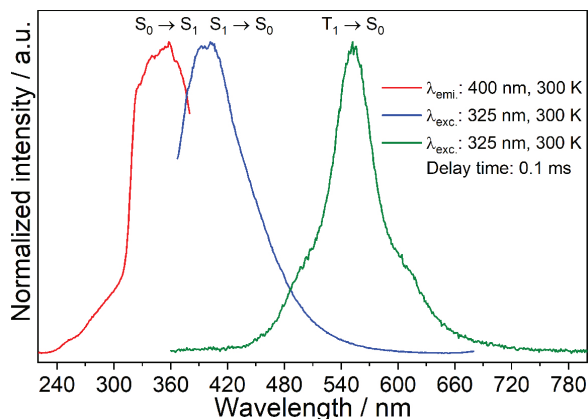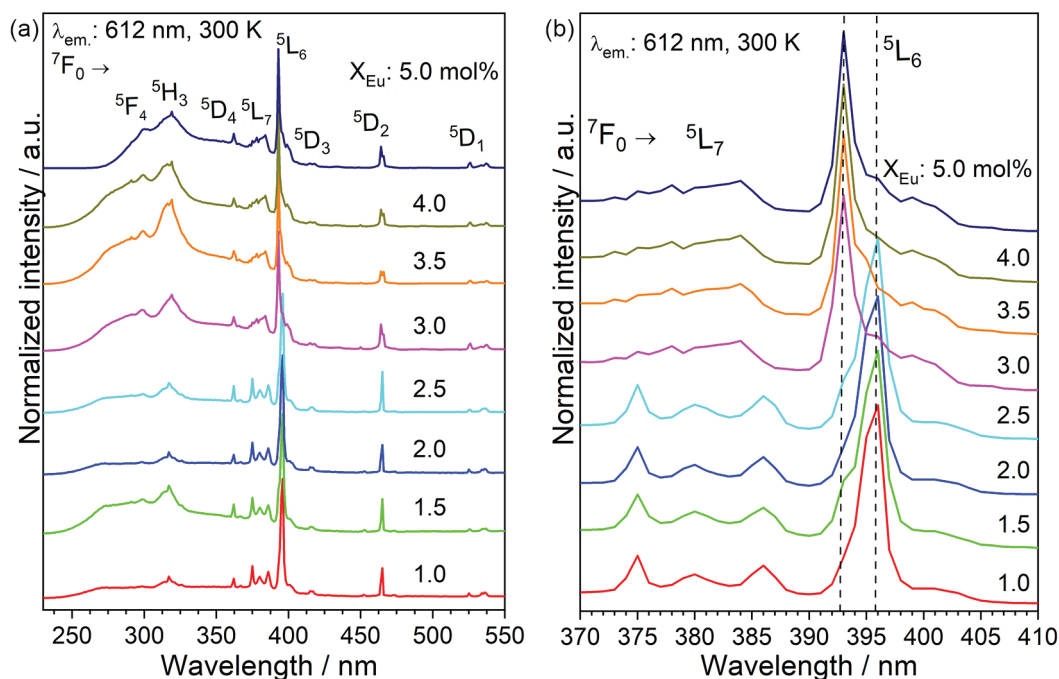
Figure 4. Excitation spectra of nondoped [Zn₃(BTC)₂·12H₂O] compound at 300 K (red curve) (monitoring at 400 nm), fluorescence (blue) and phosphorescence (green) with 0.1 ms delay time, under excitation at 325 nm (300 K).

The emission spectra of the nondoped [Zn₃(BTC)₂·12H₂O] compound under excitation at 325 nm (300 K) shows fluorescence and phosphorescence, which provided yet further information about the electronic transitions of the BTC ligand (Figure 4). Consistent with the literature,[10,14,19] these spectra revealed an intense fluorescence peak at around 400 nm (Figure 4, blue line) assigned to the radiative decay from $S_1 \rightarrow S_0$ transition of the BTC linker. Time-resolved measurements (0.1 ms of delay time) also allowed detection of phosphorescent emission by the BTC ligand (Figure 4, green line) from 460 to 640 nm (maximum intensity: 550 nm), believed to stem from the radiative decay of the first excited triplet

state ($T_1 \rightarrow S_0$). Identification of the energy signature of this triplet state (T_1) is vital for spectral analyses of the doped luminescent compounds since it is known to play a critical role in intramolecular energy transfer processes from the ligand to RE³⁺ ions.[11,21-23] Around this band at 550 nm two shoulders are observed. These two shoulders are possibly due to the vibrational structure of the triplet state of the ligand. Another possibility is that these shoulders arise from slightly different triplet states due to different structural arrangements of the six carboxylate groups from the two BTC ligands coordinated to the lanthanide ion.

Room temperature excitation spectra of doped [Zn₃(BTC)₂·12H₂O] with different Eu³⁺ concentrations (1.0-5.0 mol%) in the spectral range from 200 to 500 nm were recorded (Figure 5a). Excitation was monitored at 612 nm, corresponding to the hypersensitive $^5D_0 \rightarrow {^7F_2}$ transition of the Eu³⁺ ions. The excitation spectra consistently revealed a broad absorption band extending from 260 to 410 nm (ca. 316 nm), which originated from the sensitization of the Eu³⁺ ions by the population of the S_2 and S_1 excited states of the BTC linker. These ligand excitation bands overlapped the narrow intra-configurational 4f transition bands of Eu³⁺ ions (in cm⁻¹): $^7F_0 \rightarrow {^5F_4}$ (33300), $^5H_3$ (31546), $^5D_4$ (27624), $^5L_7$ (26810-25910) and $^5L_6$ (25445, 25252). In addition, it is observed the following 4f⁶ electronic transition (in cm⁻¹): $^5D_3$ (24096 and 23980), $^5D_2$ (21552-21459) and $^5D_1$ (19048-18622).[24,25]

The relative difference in the excitation intensity of the 4f-4f transition of the Eu³⁺ ions indicated different

Figure 5. (a) Excitation spectra of the doped [Zn₃(BTC)₂·12H₂O] with different Eu³⁺ concentrations (λ_{em} = 612 nm, 300 K); (b) amplification in the region of the $^7F_0 \rightarrow {^5L_7}$ and $^5L_6$ characteristic transitions of the Eu³⁺ ion.
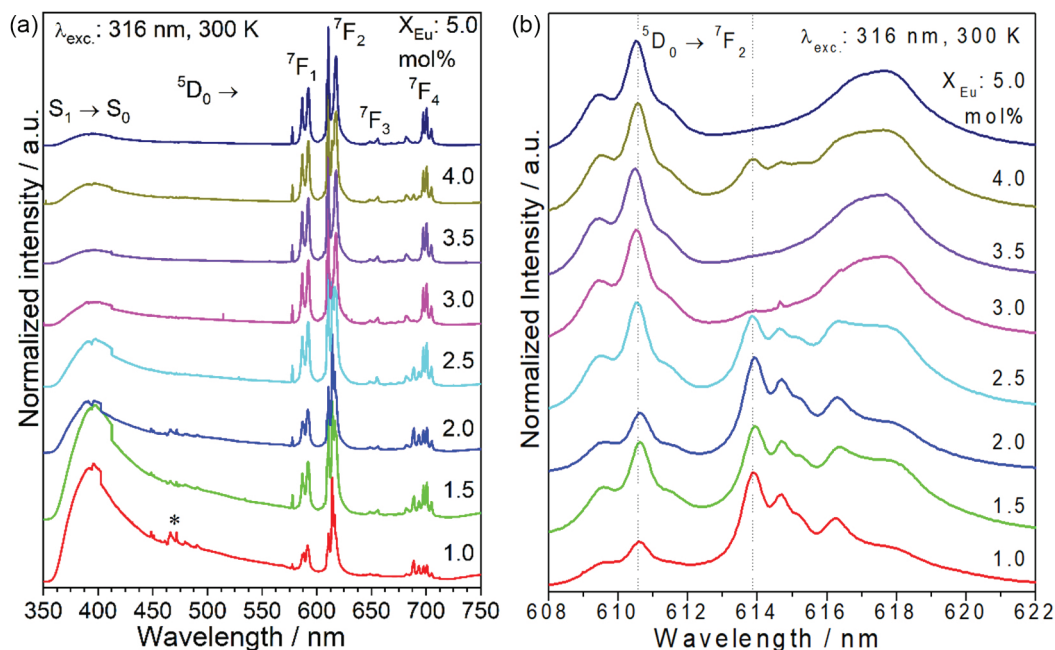
Figure 6. (a) Emission spectra of the doped $[Zn_3(BTC)_2 \cdot 12H_2O]$ with different Eu^{3+} concentrations ($\lambda_{exc} = 316$ nm, 300 K); (b) amplification in the region of the $^5D_0 \rightarrow {^7F_2}$ Eu^{3+} hypersensitive transition (*peaks of xenon lamp).

incorporation of the dopant ions within the crystal structure at different dopant concentrations (1.0, 1.5, 2.0, 2.5, 3.0, 3.5, 4.0, 4.5, and 5.0 mol%). In materials doped with lower concentrations (1.0 to 2.5 mol%), the excitation of the Eu^{3+} ion was relatively more intense compared to the materials doped with higher concentrations (3.0 to 5.0 mol%), suggesting more efficient sensitization of the emitting centers in these compounds.[11]

The emission spectra of doped $[Zn_3(BTC)_2 \cdot 12H_2O]$ MOFs (300 K, $\lambda_{exc} = 316$ nm) in Figure 6a show the fluorescence band of the BTC ligand ($S_1 \rightarrow S_0$) at around 420 nm seen in the nondoped MOF spectrum (Figure 4), even at the highest dopant concentrations. However, this band from the ligand gradually decreased in intensity relative to the characteristic transitions of the Eu^{3+} ion ($^5D_0 \rightarrow {^7F_{0-4}}$) as the concentration of the dopant increased from 1.0 to 5.0 mol%. This optical behavior indicated that excitation of the ligand at higher energy wavelengths (316 nm) produced competitive emission between the linker fluorescence ($S_1 \rightarrow S_0$) and Eu^{3+} ions luminescence. This interpretation was supported by a CIE (Commission Internationale de l'Éclairage) color coordination analysis, revealing sufficient competitive emission to induce a linear shift in the material color from ligand produced blue towards a Eu^{3+} produced red with increased doping concentration (Figure 7 and Table S5, SI section).[26]

As mentioned above, Eu^{3+} ions possess unique spectroscopic properties that allow them to act as powerful luminescent probes and chemical environment sensors. The Eu^{3+} $^5D_0 \rightarrow {^7F_2}$ transition is extremely sensitive to the
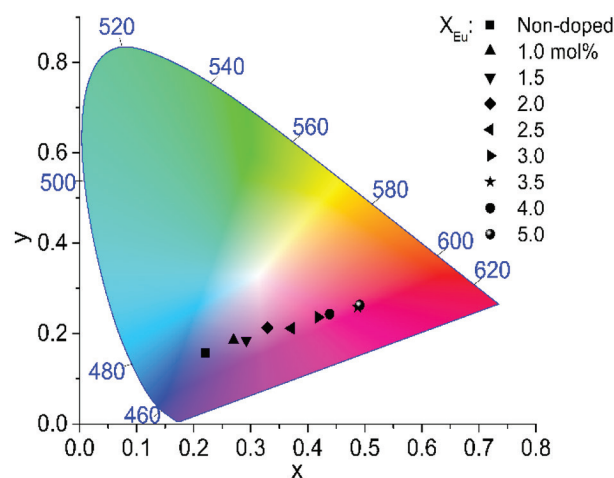
Figure 7. CIE 1931 chromaticity diagram showing the characteristic emission colors of $[Zn_3(BTC)_2 \cdot 12H_2O:Eu^{3+}]$ when excited at 316 nm.
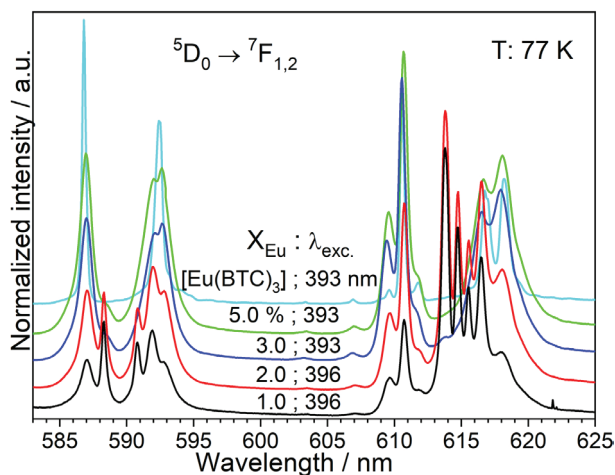
chemical environment, with its emission intensity varying considerably depending on the coordination geometry and ligand polarizability. Changes in the emission intensity of the $^5D_0 \rightarrow {^7F_2}$ transition may be compared to the $^5D_0 \rightarrow {^7F_1}$ transition, which is virtually insensitive to the environment and serves as an internal standard.[11,21-23,27]

Figure 6b presents the emission intensity of the $^5D_0 \rightarrow {^7F_2}$ transition at around 614 ($\lambda_{exc} = 316$ nm, 300 K) for the doped materials (1.0 to 5.0 mol%). The spectra for the compounds doped with concentrations between 1.0 and 2.0 mol% had maximum emission intensity located at approximately 614 nm, with the band at ca. 610 nm being relatively less intense. At a doping concentration

of 2.5 mol%, however, the two bands had comparable intensities, and when the doping concentration exceeded 2.5 mol%, the band intensity at ca. 610 nm exceeded that of the band at 614 nm. It is noteworthy that both bands were present in the spectra of all 8 MOFs.

Figure 8 and Figures S3, S4 and S5 (SI section) present the changes in the emission profiles of the doped compounds in response to variation of the excitation wavelength and the doping percentage. Here, we specifically targeted the most intense excitation band, resulting from the $^7F_0 \rightarrow {}^5L_6$ transition, in order to more accurately observe changes in emission intensity due to potential differences in symmetry profiles. A reference material, [Eu(BTC)₃], which contained only the linker BTC and Eu³⁺ ions, was synthesized under the same conditions as the [Zn₃(BTC)₂·12H₂O] compound and used as a control for these experiments (Figure S6, SI section). Each compound was excited using radiation corresponding to its maximum excitation energy (1.0-2.0 mol% Eu³⁺: 396 nm; 3.0-5.0 mol% and reference: 393 nm), to allow for accurate comparison of the individual spectra. The emission profiles of the [Zn₃(BTC)₂·12H₂O] with 3.0 and 5.0 mol% Eu³⁺ doping were found to be very similar to the reference compound [Eu(BTC)₃], while the MOFs doped with lower concentrations produced spectra that deviated more dramatically. This suggested that the majority of the emission energy produced by the compound doped with lower concentrations of Eu³⁺ comes from non-Eu³⁺ components of the crystal. As the dopant concentrations increased, however, Eu³⁺ contributed more significantly to the emission spectrum. Supporting this interpretation, closer examination of the spectra of the

[Zn₃(BTC)₂·12H₂O] doped with 1.0 and 2.0 mol% Eu³⁺ ions revealed a drop off in the intensity of the band at 614 from 2.8 times that of the band at 610 down to only 1.5 times the intensity, indicating a greater contribution of Eu³⁺ to the spectra as the doping concentration increased. Interestingly, the relatively small differences between the spectrum of the MOFs doped with 3.0 and 5.0 mol% suggests a limit for the incorporation of the Eu³⁺ ion in the structure of [Zn₃(BTC)₂·12H₂O], potentially as a result of the differences in charge and radii compared to the native Zn²⁺ ions.

In order to confirm the existence of this incorporation limit, ICP OES measurements were performed to observe the ratio between the amount of dopant and the Zn²⁺ cation within the materials. The values shown in Table S6 (SI section) indeed indicate a non-linear increase in the ratio between Eu³⁺ and Zn²⁺ in the doped MOFs, with increases in doping concentrations at lower percentages resulting in greater increases in incorporated Eu³⁺ than increases at higher percentages.

Excitation kinetics

The luminescence decay curves of the doped [Zn₃(BTC)₂·12H₂O] were fitted by two exponential curves (Figure S7, SI section), indicating the presence of two distinct decay time emissions within the compound, by using the expression $I_{(t)} = A_1 e^{(-t/\tau 1)} + A_2 e^{(-t/\tau 2)}$, where τ_1 and τ_2 are the short and long lifetimes and A_1 and A_2 are the respective intensity coefficients (Table S7, SI section). From this reasoning, we get an average lifetime ($<\tau>$) given by:[28-33]

$$<\tau> = (A_1\tau_1^2 + A_2\tau_2^2) / (A_1\tau_1 + A_2\tau_2) \qquad (1)$$

Calculated luminescence lifetimes for the doped compounds excited with different excitation energies (at 300 K) are summarized in Table 1. Direct excitation of Eu³⁺ ion at $^5L_6$ and $^5D_2$ excitation states at 393 and 464 nm, respectively, revealed marked differences in luminescence lifetimes of these transitions depending on europium doping concentration. [Zn₃(BTC)₂·12H₂O] doped compound with less than 2.5 mol% of Eu³⁺ ions exhibited considerably shorter luminescence lifetimes compared to the materials doped with concentrations above 3.0 mol%. This may be explained by the improved structural uniformity and increased pore size in materials containing fewer large, structure disrupting Eu³⁺ ions, facilitating MOF hydration. The OH-bonds within the water molecules improved non-radiative decay via vibrational coupling, facilitating decay and decreasing luminescence lifetime.

Figure 8. Emission spectra of doped-[Zn₃(BTC)₂·12H₂O] with varying concentrations of Eu³⁺ ions and reference sample [Eu(BTC)₃], monitoring the most intense excitation wavelength (393 and 396 nm), low temperature (77 K), highlighting the intra-configuration transitions $^5D_0 \rightarrow {}^7F_1$ and $^7F_2$, characteristics of the Eu³⁺ ion.

Table 1. Average lifetime of [Zn$_3$(BTC)$_2$·12H$_2$O:Eu^{3+} (x mol%)], monitoring the emission in 610 nm and in different excitation regions at 316 (S$_0$ → S$_1$), 393 (^{7}F$_0$ → ^{5}L$_6$) and 464 nm (^{7}F$_0$ → ^{5}D$_2$), at room temperature (300 K)

Doping / mol%	Lifetime ⟨τ⟩ / ms		
	316 nm	393 nm	464 nm
5.0	1.671	1.613	1.286
4.0	1.778	1.430	1.190
3.5	1.893	1.836	1.646
3.0	1.851	1.803	1.549
2.5	1.375	0.856	0.923
2.0	1.272	0.844	0.654
1.5	1.230	0.762	0.626
1.0	1.040	0.587	0.450

Differences in luminescence lifetimes were observed when the [Zn$_3$(BTC)$_2$·12H$_2$O:Eu^{3+}] materials were excited with light corresponding to the energy of the ^{7}F$_0$ → ^{5}L$_6$ transition (393 nm) rather than the ^{7}F$_0$ → ^{5}D$_2$ transition (464 nm) due to the higher excitation intensity in the former transition.

The increased luminescence lifetimes of the doped compounds excited by 316 nm in the BCT ligand compared with excitation at 393 and 464 nm in the Eu^{3+} ion the intramolecular energy transfer process is less efficient. The number of steps involved in the excitation and emission processes leads to longer luminescence lifetimes than the ones involving the direct excitation of the Eu^{3+} ions. Interestingly, comparing luminescence lifetimes of the [Eu(BTC)$_3$] MOF and doped [Zn$_3$(BTC)$_2$·12H$_2$O] compounds suggests that Eu^{3+} sensitization by BTC ligands in the [Zn$_3$(BTC)$_2$·12H$_2$O] MOF is relatively less efficient, which explains the duration of luminescent lifetimes for these MOFs even further (Table S7, SI section).

Finally, the reversal of the relationship between the duration of luminescence lifetime and doping concentration that occurs MOFs at a doping concentration of 3.5 mol% may be explained by the quenching by concentration phenomenon. This probably occurs when luminescent of europium ions are present at high enough concentrations to allow energy retro-transfer between individual ions, which increases the capacity of the compound to utilize non-radiative decay pathways, suppressing the emission of the material and reducing the time which excited levels remain populated.[18,34]

Experimental intensity parameters

Experimental intensity parameters (Ω$_λ$) of the Eu^{3+} ion serve as a marker for the local geometry, coordinate atoms, and polarizability in its first coordination sphere.

Here we calculated the values of Ω$_2$ (a marker of small angular changes in the local coordination geometry) and Ω$_4$ (a marker of bond length and covalence) for the doped [Zn$_3$(BTC)$_2$·12H$_2$O] MOFs to reveal information about their structures.[35] This was done using a series of calculations utilizing data from the emission spectra analysis of these compounds, beginning with emission intensity.

The emission intensity (I) of the transitions between the ^{5}D$_0$ emitter level and the acceptor levels ^{7}F$_J$ (J = 0, 1, 2, 3 and 4) of the Eu^{3+} ion is expressed by the equation:

$$I = A_{rad} N_0 \tag{2}$$

where A$_{rad}$ is the Einstein spontaneous emission coefficient, and N$_0$ is the population of the ^{5}D$_0$ emitter level. The spontaneous emission coefficient for the transition from a level J to J' (A$_{J→J'}$) is represented by equation 3:

$$A_{J \to J'} = \frac{4e^2 \omega_{J \to J'}^3}{3\hbar c^3 (2J+1)} \left[\frac{n(n^2+2)^2}{9} \sum_\lambda \Omega_\lambda \left\langle \alpha J \left\| U^{(\lambda)} \right\| \alpha'J' \right\rangle^2 + \frac{n^3 \hbar^2}{4m^2 c^2} \left\langle \alpha J \left\| L+2S \right\| \alpha'J' \right\rangle^2 \right] \tag{3}$$

where e is the charge of the electron, m is the electron mass, c is the speed of light, ω$_{J→J'}$ is the angular frequency of the transition αJ→α'J', $\sum_\lambda \Omega_\lambda \left\langle \alpha J \left\| U^{(\lambda)} \right\| \alpha'J' \right\rangle^2$ e^2 is the electric dipole force, $\left\langle \alpha J \left\| L+2S \right\| \alpha'J' \right\rangle^2$ e^2 is the magnetic dipole force and the Ω$_λ$'s are the 4f-4f intensity parameters.[36,37]

The value of A$_{0→J}$ for Eu^{3+}-containing compounds can be determined by analyzing experimental data generated by emission spectra and using the ^{5}D$_0$ → ^{7}F$_1$ emission bands as an internal standard. Incorporating this comparison in equation 4 generates the expression:[11,36]

$$A_{0 \to J} = \left(\frac{S_{0 \to J}}{S_{0 \to 1}} \right) A_{0 \to 1} \tag{4}$$

where S is the integral under the emission bands for the ^{5}D$_0$ → ^{7}F$_{0,1,2,3,4}$ transitions.[38] This expression should be used for experimental measurements of the number of photon counting. If the measurements are in emitted power, then in equation 4 the ration between emitted energies must be included. Since the emission rate for ^{5}D$_0$ → ^{7}F$_1$ transition is essentially constant, the Einstein coefficient A$_{0→1}$ can be calculated by taking A$_{0→1}$ = 0.31 × 10^{-11} n^3 (σ$_{0→1}$)^3. We assume the index of refraction n = 1.5 for Eu^{3+} solid-state samples. This procedure is consistent only for the trivalent europium ion.

The intensity parameters Ω$_2$ and Ω$_4$ can be determined from the respective spontaneous emission values (A$_{0→λ}$) according to the expression:

$$\Omega_\lambda = \frac{3\hbar c^3 A_{0\to\lambda}}{4e^2\omega^3\chi \left\langle {}^7_x F_\lambda \left\| U^{(\lambda)} \right\| {}^5 D_0 \right\rangle^2} \qquad (5)$$

where $\chi = n\,(n^2 + 2)^2 / 9$ is the Lorentz correction term for the local field and $\left\langle {}^7_x F_\lambda \left\| U^{(\lambda)} \right\| {}^5 D_0 \right\rangle^2$ is the square of the doubly reduced matrix element and takes on the values 0.0032; 0.0023 and 0.0002 for $\lambda = 2$, 4 and 6, respectively.[25,38] This work does not address the value of Ω_6 since no data for the ${}^5D_0 \to {}^7F_6$ transition was collected.

The intrinsic quantum yield of europium compounds (quantum efficiency or internal quantum efficiency) of a ${}^5D_0$ emitting level ($Q_{Eu^{3+}}^{Eu^{3+}}$), defined previously, depends on the radiative (A_{rad}) and non-radiative (A_{nrad}) rates due to multiphonon deactivation processes of the emitting level given by:

$$Q_{Eu^{3+}}^{Eu^{3+}} = \frac{A_{rad}}{A_{rad} + A_{nrad}} \qquad (6)$$

For doped [Zn₃(BTC)₂·12H₂O:Eu³⁺] MOFs, the values of A_{rad} are determined by the sum of the radiative contributions of the Eu³⁺ transitions ($A_{rad} = \Sigma_{J=1,2,4}A_{0\to J}$) and the values of A_{tot} are calculated from the luminescence lifetime of the ${}^5D_0$ emitter state, using the expression $A_{tot} = 1/\tau = A_{rad} + A_{nrad}$. Using equations 2 to 5 and the optical measurements obtained from the emission spectra (Figure S8, SI section), A_{rad}, A_{nrad}, Ω_2 and Ω_4 and $Q_{Eu^{3+}}^{Eu^{3+}}$ were determined for the [Zn₃(BTC)₂·12H₂O:Eu³⁺] MOFs and are presented in Table 2.

The higher values of Ω_2 parameter obtained for the compounds with doping concentration less than 2.5 mol% of Eu³⁺ ions suggested a relatively low centrosymmetric character around these ions, compared to the materials

doped with higher Eu³⁺ concentrations, as Ω_2 tends rapidly towards zero for highly centrosymmetric sites.[36]

The decrease in Ω_4 values observed with increasing doping concentration suggested a decrease in bond length and bond polarization with an increase in Eu³⁺ concentration in the crystal structure of the [Zn₃(BTC)₂·12H₂O:Eu³⁺] system.[38,39]

The non-radiative emission rates (A_{nrad}) indicated in Table 2 show that materials doped with less than 2.5 mol% of Eu³⁺ ions have higher energy losses through non-radiative decay, suggesting greater multiphonon relaxation and more water molecules in the first coordinate sphere of these compounds. Though [Zn₃(BTC)₂·12H₂O] doped with concentrations higher than 3.0 mol% had considerably lower non-radiative decay rates. Therefore, there was a slight increase in energy loss with increased doping concentration, probably as a result of concentration quenching.

The intrinsic quantum yield ($Q_{Eu^{3+}}^{Eu^{3+}}$) of the compounds increased with increased doping concentration from 1.0 to 3.0 mol%, then reversed, decreasing until 5.0 mol%, though never reaching values as low as those obtained for 1.0 mol% doping (Table 2). It is noteworthy that the quantum efficiency of all these [Zn₃(BTC)₂·12H₂O] MOFs were higher than [Eu(BTC)₃·6H₂O] hydrated MOF produced by the co-precipitation method ($Q_{Eu^{3+}}^{Eu^{3+}} = 12\%$).[35] It is observed from Table 2 that the non-radiative decay values (A_{nrad}) are considerably higher than the radiative decays (A_{rad}). This is due to the presence of the water molecules in MOF structure, through vibronic coupling with the OH oscillators.

Conclusions

The hydrothermal synthesis assisted by microwave heating led to the [Zn₃(BTC)₂·12H₂O] compound with high crystallinity and shorter reaction time, using only

Table 2. Experimental intensity parameters (Ω_λ), $Q_{Eu^{3+}}^{Eu^{3+}}$, A_{nrad}, A_{rad} and A_{tot} rates at the room temperature for the compounds [Zn₃(BTC)₂·12H₂O:Eu³⁺ (x mol%)] produced by the microwave assisted hydrothermal method

Doping concentration / mol%	Ω_2 / (10^{-20} cm²)	Ω_4 / (10^{-20} cm²)	A_{rad} / s⁻¹	A_{nrad} / s⁻¹	A_{tot} / s⁻¹	$Q_{Eu^{3+}}^{Eu^{3+}}$ / %
5.0	3.6	2.6	199	420	619	32
4.0	3.9	2.6	206	494	700	30
3.5	3.5	2.6	195	350	545	36
3.0	3.9	2.8	208	340	548	38
2.5	5.3	3.8	269	899	1168	23
2.0	4.7	3.3	244	941	1185	21
1.5	5.5	4.2	278	1033	1311	21
1.0	5.0	3.7	257	1447	1704	15

Ω_2: marker of small angular changes in the local coordination geometry; Ω_4: marker of bond length and covalence; A_{rad}: radiative rate; A_{nrad}: non-radiative rate; A_{tot}: total emission rate; $Q_{Eu^{3+}}^{Eu^{3+}}$: intrinsic quantum yield.

water as the solvent. The fast crystallization of this MOF allowed the study of the *in situ* incorporation of Eu^{3+} ions, despite the difference of charge and radius between the Zn^{2+} and Eu^{3+} ions, which make this substitution difficult in the same symmetry site without any distortion of the coordination network. The incorporation of the dopant ion in percentages from 1.0 to 5.0 mol% led to a change in the emission color ranging from blue to red according to the increase of Eu^{3+} ion concentration. The characteristic spectroscopic properties of the Eu^{3+} ion allowed to differentiate the location of this ion in two different sites of symmetry, having different contributions to the emission of the materials, according to the increase of the doping concentration. This result indicated higher phase segregation in doping above 3.0 mol% of Eu^{3+} ions, due to the change in emission profile and the intensity ratio between the $^5D_0 \rightarrow {}^7F_2$ and $^7F_1$ transitions.

The emission profile observed in doping concentrations higher than 3.0 mol% resembled the emission of the $[Eu(BTC)_3]$ compound, suggesting the formation of this species when incorporation limit of the dopant ion to MOF $[Zn_3(BTC)_2 \cdot 12H_2O]$ was reached. Even though there is no very efficient energy transfer between the ligand-to-metal, we could observe the emission color tuning originated from the emissions of the BTC ligand (blue) and Eu^{3+} ion (red).

Supplementary Information

Supplementary information is available free of charge at http://jbcs.sbq.org.br as PDF file.

Acknowledgments

References

1. Rowsell, J. L. C.; Yaghi, O. M.; *Microporous Mesoporous Mater.* **2004**, *73*, 3; Yaghi, O. M.; O'Keeffe, M.; Ockwig, N. W.; Chae, H. K.; Eddaoudi, M.; Kim, J.; *Nature* **2003**, *423*, 705.

2. Férey, G.; *Chem. Soc. Rev.* **2008**, *37*, 191.

3. Hasegawa, Y.; Nakanishi, T.; *RSC Adv.* **2015**, *5*, 338.

4. Deacon, G.; *Coord. Chem. Rev.* **1980**, *33*, 227.

5. Allendorf, M. D.; Bauer, C. A.; Bhakta, R. K.; Houk, R. J. T.; *Chem. Soc. Rev.* **2009**, *38*, 1330.

6. Cui, Y.; Yue, Y.; Qian, G.; Chen, B.; *Chem. Rev.* **2012**, *112*, 1126.

7. Hu, Z.; Deibert, B. J.; Li, J.; *Chem. Soc. Rev.* **2014**, *43*, 5815.

8. Friend, R. H.; Gymer, R. W.; Holmes, A. B.; Burroughes, J. H.; Marks, R. N.; Taliani, C.; Bradley, D. D. C.; dos Santos, D. A.; Brédas, J. L.; Lögdlund, M.; Salaneck, W. R.; *Nature* **1999**, *397*, 121; Gao, C.; Xiong, Z.; Yu, F.; Ma, X.; Zhang, Y.; Zeng, X.; Xiong, Z.; *Opt. Photonics J.* **2017**, *07*, 99; Hagan, A. K.; Zuchner, T.; *Anal. Bioanal. Chem.* **2011**, *400*, 2847; Laukkanen, M.-L.; Orellana, A.; Keinänen, K.; *J. Immunol. Methods* **1995**, *185*, 95; Law, G.-L.; Wong, K.-L.; Tam, H.-L.; Cheah, K.-W.; Wong, W.-T.; *Inorg. Chem.* **2009**, *48*, 10492; Lestari, W. W.; Lönnecke, P.; Streit, H. C.; Handke, M.; Wickleder, C.; Hey-Hawkins, E.; *Eur. J. Inorg. Chem.* **2014**, *2014*, 1775; Liang, B.; Jiang, C.; Chen, Z.; Zhang, X.; Shi, H.; Cao, Y.; *J. Mater. Chem.* **2006**, *16*, 1281; Rodrigues, C. V.; Luz, L. L.; Dutra, J. D. L.; Junior, S. A.; Malta, O. L.; Gatto, C. C.; Streit, H. C.; Freire, R. O.; Wickleder, C.; Rodrigues, M. O.; *Phys. Chem. Chem. Phys.* **2014**, *16*, 14858; Vasilopoulou, M.; Georgiadou, D.; Pistolis, G.; Argitis, P.; *Adv. Funct. Mater.* **2007**, *17*, 3477; Weber, I. T.; de Melo, A. J. G.; Lucena, M. A. M.; Rodrigues, M. O.; Alves, S.; *Anal. Chem.* **2011**, *83*, 4720.

9. Yaghi, O. M.; Li, H.; Groy, T. L.; *J. Am. Chem. Soc.* **1996**, *118*, 9096.

10. Majumder, A.; Shit, S.; Choudhury, C. R.; Batten, S. R.; Pilet, G.; Luneau, D.; Daro, N.; Sutter, J.-P.; Chattopadhyay, N.; Mitra, S.; *Inorg. Chim. Acta* **2005**, *358*, 3855.

11. Brito, H. F.; Malta, O. M. L.; Felinto, M. C. F. C.; Teotonio, E. E. S. In *PATAI'S Chemistry of Functional Groups*; Rappoport, Z.; Zabicky, J., eds.; John Wiley & Sons, Ltd.: Hoboken, 2009, p. 131-184.

12. Cunha, C. S.; Köppen, M.; Terraschke, H.; Friedrichs, G.; Malta, O. L.; Stock, N.; Brito, H. F.; *J. Mater. Chem. C* **2018**, *6*, 12668; Rönfeldt, P.; Reinsch, H.; Faßheber, N.; Terraschke, H.; Stock, N.; *Eur. J. Inorg. Chem.* **2020**, *2020*, 1147; Rönfeldt, P.; Ruser, N.; Reinsch, H.; Grape, E. S.; Inge, A. K.; Suta, M.; Terraschke, H.; Stock. N.; *Eur. J. Inorg. Chem.* **2020**, *28*, 2737; Terraschke, H.; Ruiz Arana, L.; Lindenberg, P.; Bensch, W.; *Analyst* **2016**, *141*, 2588; Terraschke, H.; Rothe, M.; Tsirigoni, A.-M.; Lindenberg, P.; Ruiz Arana, L.; Heidenreich, N.; Bertram, F.; Etter, M.; *Inorg. Chem. Front.* **2017**, *4*, 1157; Zhang, J.; Cai, G.; Wang, W.; Ma, L.; Wang, X.; Jin, Z.; *Inorg. Chem.* **2020**, *59*, 2241; Li, G. H.; Yang, N.; Guo, J. G.; Wang, Z. L.; Cai, G. M.; Wang, X. J.; *Dalton Trans.* **2020**, *49*, 3260.

13. Shannon, R. D.; *Acta Crystallogr., Sect. A: Found. Adv.* **1976**, *32*, 751.

14. Zou, X.; Zhu, G.; Hewitt, I. J.; Sun, F.; Qiu, S.; *Dalton Trans.* **2009**, 3009.

15. Pavia, D. L.; *Introduction to Spectroscopy*, 4th ed.; Brooks/Cole, Cengage Learning: Belmont, CA, USA, 2009.

16. Nakamoto, K.; *Infrared and Raman Spectra of Inorganic and Coordination Compounds*, 6th ed.; Wiley: Hoboken, NJ, USA, 2009.

17. Silverstein, R. M.; Webster, F. X.; Kiemle, D. J.; *Spectrometric Identification of Organic Compounds*, 7th ed.; Wiley: Hoboken, NJ, USA, 2005.

18. Marciniak, L.; Hreniak, D.; Strek, W.; *J. Mater. Chem. C* **2014**, *2*, 5704.

19. Qiu, L.-G.; Li, Z.-Q.; Wu, Y.; Wang, W.; Xu, T.; Jiang, X.; *Chem. Commun.* **2008**, 3642.

20. Güler, S. H.; Güler, Ö.; Evin, E.; Islak, S.; *Optik* **2016**, *127*, 3187; Sivula, K.; Zboril, R.; Le Formal, F.; Robert, R.; Weidenkaff, A.; Tucek, J.; Frydrych, J.; Grätzel, M.; *J. Am. Chem. Soc.* **2010**, *132*, 7436; Tauc, J.; *Mater. Res. Bull.* **1968**, *3*, 37.

21. Binnemans, K.; *Coord. Chem. Rev.* **2015**, *295*, 1.

22. Bünzli, J.-C. G.; Choppin, G. R.; *Lanthanide Probes in Life, Chemical and Earth Sciences*; Elsevier: Amsterdam, 1989.

23. Bünzli, J.-C. G.; *Coord. Chem. Rev.* **2015**, *293-294*, 19.

24. Kodaira, C. A.; Brito, H. F.; Malta, O. L.; Serra, O. A.; *J. Lumin.* **2003**, *101*, 11; Kubota, S.-I.; Izumi, M.; Yamane, H.; Shimada, M.; *J. Alloys Compd.* **1999**, *283*, 95; Shi, F.; Meng, J.; Ren, Y.; Su, Q.; *J. Phys. Chem. Solids* **1998**, *59*, 105; Yamase, T.; Kobayashi, T.; Sugeta, M.; Naruke, H.; *J. Phys. Chem. A* **1997**, *101*, 5046.

25. Carnall, W. T.; Crosswhite, H.; Crosswhite, H. M.; *Energy Level Structure and Transition Probabilities of the Trivalent Lanthanides in LaF₃*; Argonne National Laboratory: Lemont, IL, USA, 1977.

26. Krishnaprasad, K.; Raheem, S.; Vijayalekshmi, P.; Kamalasastri, C.; *Talanta* **1996**, *43*, 1187; Santa-Cruz, P. A.; Teles, F. S.; *SpectraLux Software v. 2.0*; Ponto Quântico Nanodispositivos, Recife, PE, Brazil, 2003.

27. de Sousa Filho, P. C.; Lima, J. F.; Serra, O. A.; *J. Braz. Chem. Soc.* **2015**, *26*, 2471.

28. Taylor, K. M. L.; Jin, A.; Lin, W.; *Angew. Chem., Int. Ed.* **2008**, *47*, 7722.

29. Yardley, J. T. In *Introduction to Molecular Energy Transfer*; Yardley, J. T., ed.; Academic Press: New York, 1980, p. 189-204.

30. Lakowicz, J. R.; *Principles of Fluorescence Spectroscopy*, 3rd ed.; Springer: New York, 2010.

31. Murakami, S.; Herren, M.; Rau, D.; Morita, M.; *Inorg. Chim. Acta* **2000**, *300-302*, 1014.

32. Tanaka, F.; Ishibashi, T.; *Faraday Trans.* **1996**, *92*, 1105.

33. Som, S.; Mitra, P.; Kumar, V.; Terblans, J. J.; Swart, H. C.; Sharma, S. K.; *Dalton Trans.* **2014**, *43*, 9860.

34. Haas, Y.; Stein, G.; *J. Phys. Chem.* **1972**, *76*, 1093.

35. Silva, I. G. N.; Mustafa, D.; Andreoli, B.; Felinto, M. C. F. C.; Malta, O. L.; Brito, H. F.; *J. Lumin.* **2016**, *170*, 364; Moura, R. T.; Carneiro Neto, A. N.; Longo, R. L.; Malta, O. L.; *J. Lumin.* **2016**, *170*, 420.

36. de Sá, G. F.; Malta, O. L.; Donegá, C. M.; Simas, A. M.; Longo, R. L.; Santa-Cruz, P. A.; da Silva, E. F.; *Coord. Chem. Rev.* **2000**, *196*, 165.

37. Judd, B. R.; *J. Chem. Phys.* **1979**, *70*, 4830.

38. Teotonio, E. E. S.; Fett, G. M.; Brito, H. F.; Faustino, W. M.; de Sá, G. F.; Felinto, M. C. F. C.; Santos, R. H. A.; *J. Lumin.* **2008**, *128*, 190.

39. Ferreira, R. A. S.; Nobre, S. S.; Granadeiro, C. M.; Nogueira, H. I. S.; Carlos, L. D.; Malta, O. L.; *J. Lumin.* **2006**, *121*, 561.